RSC Advances

PAPER

View Article Online
View Journal | View Issue

Cite this: *RSC Adv.*, 2019, **9**, 33997

Boosting the hydrogen evolution activity of a Co–N–C electrocatalyst by codoping with Al†

Xiao Zhou, Haoran Yu, Yang Liu, Yong Kong, Yongxin Tao and Yong Qin *

Co, Al and N tri-doped graphene (CANG) was successfully fabricated *via* annealing N-doped graphene with Co and Al precursors. The material was characterized by scaning electron microscopy (SEM), transmission electron microscopy (TEM), X-ray diffraction (XRD), Raman spectroscopy, physical adsorption, and X-ray photoelectron spectroscopy (XPS). It was found that the as-prepared CANG features a robust three-dimensional hierarchically porous structure. The contents of Co and Al can achieve the maximum value of 2.18 at% and 0.51 at% at the annealing temperature of 950 °C. Upon using the electrocatalyst for the hydrogen evolution reaction (HER), the CANG exhibited remarkable electrocatalytic performance in both acidic (η_{10} = 105 mV) and alkaline media (η_{10} = 270 mV), and outperforms Co,N-codoped graphene and Al,N-codoped graphene, respectively. In combination with the density functional theory (DFT) calculations, it was revealed that the introduction of the Al heteroatom can decrease the absolute value of hydrogen adsorption free energy (ΔG(H*)) of Co–N–C catalysts, thus greatly enhancing the HER activity. This discovery will provide new guidance to the design of advanced and inexpensive carbon materials for fuel cell, water-splitting and other electrochemical devices.

Received 30th September 2019
Accepted 16th October 2019

DOI: 10.1039/c9ra07939d

rsc.li/rsc-advances

1. Introduction

The use of renewable energy such as wind and solar energy has become more and more attractive because of the ever-increasingly serious environmental pollution and the shortage of fossil fuel. Wind and solar energies can theoretically meet the major share of human demands, however, they are intrinsically intermittent.[1,2] Hydrogen is an interesting energy carrier for the storage of wind and solar energies by electrolytic or photo water splitting. Among them, electrochemical water-splitting is a preferred method for fast and large-scale hydrogen-production.[3–5] As a cathodic reaction in electrochemical water-splitting, the hydrogen evolution reaction (HER) is the pivotal process for electrolysers, and mostly depends on electrocatalysts to reduce hydrogen from water energy-efficiently and economically. Currently, Pt-based materials are the state-of-the-art electrocatalysts for HER, but the high price, scarcity and instability as well as poisoning challenges the feasibility of Pt for industrial application.[6–8] Therefore, the development of active and inexpensive electrocatalysts for the HER is highly desirable. Up to now, several classes of catalysts derived from earth-abundant elements such as transition metal carbides,[9,10] nitrides,[11,12] phosphide,[13,14] chalcogenides,[15] and selenides[16] have gained much attention, however, their inferior activity and corrosion in acid or alkaline media make them impractical for commercialization.

In recent years, carbon materials have been extensively studied as electrocatalysts, with their high electro-conductivity, low price, abundant supply, and good resistance to acid and alkaline.[17] The pure carbon merely shows extremely weak electrocatalytic activity. Heteroatom-doping is generally an efficient way to promote the electrocatalytic performance of carbon.[18,19] Particularly, transitional (*i.e.*, Fe, Co, Ni, Mo, Cu, *etc.*) and nitrogen codoped carbon (Me–N–C) materials have shown their promising future in energy-related reactions such as oxygen reduction reaction (ORR),[20,21] oxygen evolution reaction (OER),[22] and HER.[23,24] The carbon matrix can facilitate the transportation of electrons, while the nitrogen dopant can induce structural defects that strengthen the interaction with metal atoms to activate reactants. Among them, Co- and N- codoped carbon materials (*i.e.*, graphene, carbon nanotube, and active carbon) have shown their great potentials in electrocatalyzing HER.[25,26] It has been known that CoC_xN_y moiety is the active site and plays critical role in catalysing HER.[27] Albeit great progress has been achieved on Co–N–C catalysts in recent years, they still suffer from the ordinary HER activity. Certainly, the HER activity of Co–N–C catalysts can be improved by loading active nano-catalysts (*i.e.*, Co–CoO,[28] Co_3C,[29] Ni_2P[30]) on them, but the improvement by this way is usually quite limited. Very recently, it was discovered that doping a tertiary heteroatom such as sulfur[31] or phosphorous[32] is a more effective strategy to promote

Jiangsu Key Laboratory of Advanced Catalytic Materials and Technology, School of Petrochemical Engineering, Changzhou University, Changzhou, Jiangsu, 213164, China. E-mail: qinyong@cczu.edu.cn

† Electronic supplementary information (ESI) available: The Experimental section, the XPS survey and the ORR activity of CANG, the EIS and comparison of electrochemical performance of CANG with those Co–N–C catalysts reported in literature. See DOI: 10.1039/c9ra07939d

the HER activity of Co–N–C catalysts, which offers the possibility of enhancing their HER performance by tuning the structure of active centre.

In our previous works, we have proposed an Al,N-codoped three-dimensional (3D) graphene (ANG)[33] and a Co,N-codoped 3D graphene (CNG).[34] Of the two materials, ANG expressed super electrocatalytic ORR performance, unfortunately, poor HER activity.[33] In contrast, CNG showed the good HER activity, however, poor ORR performance.[34] Here, we were inspired to fabricate Co, Al, and N tri-doped 3D graphene (CANG) to create a bi-functional electrocatalyst with balanced ORR and HER performance, unexpectedly, the CANG exhibited the remarkable HER performance superior to CNG and ANG in both acid and alkaline medium. In combination with density functional theory (DFT) calculation, it was confirmed that the introduction of Al heteroatom can greatly improve the intrinsic HER activity of Co–N–C catalyst.

2. Experimental

2.1 Chemical reagents

Natural graphite powder (325 meshes) was purchased from Qingdao Graphite Co., Ltd. (Qingdao, China). Cobalt nitrate was purchased from Shanghai Qiangshun Chemical Reagent Co., Ltd. Aluminum iso-propoxide was purchased from Shanghai Runjie Chemical Reagent Co., Ltd. Formaldehyde aqueous solution (35 wt%), melamine, vitriol, phosphoric acid, and potassium permanganate were obtained from Aladdin Chemical Reagent Co., Ltd. (Shanghai, China). All other reagents not mentioned were of analytical grade and used as received.

2.2 Fabrication materials

2.2.1 Preparation of NG. Firstly, graphite flakes (1.0 g) and $KMnO_4$ (6.0 g) were added into a mixture of 120 mL concentrated H_2SO_4 and 13.3 mL H_3PO_4, producing a slight exotherm to 35 °C. The mixture was then heated at 50 °C for 12 h. The mixture was cooled to room temperature and poured into ice water (150 mL) with 30% H_2O_2 (10 mL), and then sifted through a polyester fibre. The filtrate was centrifuged (4000 rpm for 4 h), and the supernatant was decanted away. The remained solid was then washed in succession with 200 mL of water, 200 mL of 30% HCl, and 200 mL of ethanol. The solid was vacuum-dried overnight at room temperature, resulting 1.8 g GO. Secondly, 150 mg GO was dispersed in 15 mL water to produce a concentrated GO suspension, which was then mixed with 1 mL formaldehyde solution (37 wt%) and 0.35 g melamine. The dispersion was transferred into an autoclave and hydrothermally treated at 180 °C for 12 h. The obtained composite hydrogel was dried at 80 °C for 24 h in an oven. The dry aerogel was subsequently calcined at 750 °C for 5 h in N_2 atmosphere, resulting in the eventual NG product.

2.2.2 Preparation of CANG, ANG and CNG. For the preparation of CANG, 0.04 g of NG, 0.04 g of $Co(NO_3)_2$ and 0.04 g of aluminium isopropanol were dispersed in mixed solution of 10 mL H_2SO_4 and 10 mL H_2O. Then magnetic stirred the mixture for three hours. The obtained composite hydrogel was dried at 80 °C for 24 h in an oven. The dry aerogel was subsequently annealed at 950 °C for 3 h in Ar atmosphere, and leached by acid (1 M H_2SO_4, 80 °C) and alkali (1 M KOH, 80 °C) until it lost magnetism completely. The final product was denoted as CANG. For the preparation of CNG and ANG, the fabricating process is same as that of CANG, except that the precursors what they used is $Co(NO_3)_2$ or aluminium isopropanol, respectively.

2.2.3 Electrochemical measurements. The electrochemical measurements were conducted on an electrochemical cell with conventional three-electrode system. The commercial glass carbon electrode (GCE) with the diameter of 5 mm was used as the working electrode. The current densities were normalized by the geometric surface area of the GCE. The graphite rod electrode and the saturated calomel electrode (SCE) served as the counter electrode and the reference electrode, respectively. The working electrodes were fabricated by the following procedure: the suspensions (catalysts in water, 2.0 mg mL^{-1}, 10 μL) of the as-prepared materials were drop coated onto a glassy carbon disk with the diameter of 3 mm (mass loading ~0.28 mg cm^{-2}) and dried at room temperature in air for 6 h. Then 5 μL Nafion solution (0.02 wt%) were cast on the electrode surface to adhere the materials on electrodes. The potential *versus* saturated calomel electrode were converted into the potential *versus* reversible hydrogen electrode (RHE) according $E_{vs.\ \mathrm{RHE}} = E_{vs.\ \mathrm{SCE}} + E^{\theta}_{\mathrm{SCE}} + 0.059\ \mathrm{pH}$.

The calibration test was conducted in a 0.25 M H_2SO_4 solution containing 10 mM $CuSO_4$ with saturated N_2 during the whole test. The electrode was first cycled between 0.23 and 0.7 V in 0.25 M H_2SO_4 with scan speed of 10 mV s^{-1} for many scans as the background. Then the solution was changed into 0.25 M H_2SO_4 and 10 mM $CuSO_4$ with scan speed of 10 mV s^{-1}. And the electrochemical active area (ECSA) was calculated after 20 times CV scan using the following formula:

$$\mathrm{ECSA}\left(\mathrm{cm}^2\ \text{metal per g metal}\right) = \frac{Q_{\mathrm{Cu}}}{M_{\mathrm{metal}} \times 420\ \mu\mathrm{C\ cm}^{-2}} \quad (1)$$

The M_{metal} is the loading of Co on the working electrode, and Q_{Cu} is the average charge calculated from area under the voltagram of the Cu-upd CV curve.

Afterwards, the HER turnover frequency (TOF) is defined as:

$$\mathrm{TOF} = \frac{\text{total hydrogen turnovers}\Big/\mathrm{cm}_{\mathrm{geo}}^{-2}}{\text{total active sites}\Big/\mathrm{cm}_{\mathrm{geo}}^{-2}} \quad (2)$$

The upper hydrogen turnovers per geometric electrode area can be calculated by the hydrogen evolution current density under a constant overpotential:

$$\begin{aligned} \mathrm{H_2} &= \left(j\frac{\mathrm{mA}}{\mathrm{cm}_{\mathrm{geo}}{}^2}\right) \times \left(\frac{1\ \mathrm{C\ s^{-1}}}{1000\ \mathrm{mA}}\right) \times \left(\frac{1\ \mathrm{mol\ e^-}}{96\,485\ \mathrm{C}}\right) \\ &\quad \times \left(\frac{1\ \mathrm{mol\ H_2}}{2\ \mathrm{mol\ e^-}}\right) \times 6.02 \times 10^{23} \\ &= j \times 3.12 \times 10^{15}\ \mathrm{H_2}\Big/\mathrm{s^{-1}\ cm}_{\mathrm{geo}}{}^{-2} \end{aligned} \quad (3)$$

The total active sites per geometric electrode area can be calculated through the pre-calculated ECSA above.

Electrocatalytic performance measurements were conducted in a three-electrode cell using an Ag/AgCl electrode (calibrated and converted to a reverse hydrogen electrode, RHE) as the reference electrode, graphite rod electrode as the counter electrode, and the sample modified glassy carbon electrode as the working electrode.

The chronopotentiometry (*i–t*) and cycled LSV were tested in the 0.5 M H_2SO_4 solution saturated with N_2. The constant potential technique used for *i–t* test, the potential with a current density of 10 mA cm^{-2} was selected, and the speed was set to 1600 rpm min^{-1}. The test time was 20 000 seconds. For the cycle stability, the test was the LSV curve experienced 20 000 cycles.

For the cyclic voltammetry (CV) test, an O_2 flow was maintained over the electrolyte during the recording of CVs. Before data were recorded, the working electrode was cycled at least 5 times at a scan rate of 10 mV s^{-1}. For comparison, CV measurements were also carried out in N_2-saturated KOH solution. For RDE measurement, the working electrode was scanned at a rate of 10 mV s^{-1} with various rotating speed from 400 to 2400 rpm.

SCN^- tests were conducted in the solution of 0.5 M H_2SO_4 containing 10 mmol KSCN.

3. Results and discussion

3.1 The fabrication and characterization of CANG

As illustrated in Fig. 1, the CANG was prepared by a heat-treating process of 3D N-doped graphene (NG) with Al and Co precursors. The NG was firstly prepared through the method reported by us previously.[35] It had been proved that the NG possesses robust 3D structure and abundant nitrogen heteroatom (~8 at%) as well as hierarchical pore. Al and Co was secondly doped into graphene by a post heat-treatment of isopropyl aluminium and cobalt nitrate with NG.

The morphologies of CANG were firstly characterized with scan electron microscope (SEM) and transmission electron microscope (TEM), as shown in Fig. 2. SEM images clearly show the well-defined 3D interconnected network constructed by the partially overlapping graphene sheets, and continuous macroporous architecture with the pore size ranged from submicrometer to several micrometers (Fig. 2a and b), which is identical to our previously reported CNG and ANG.[33,34] TEM images further validated the 3D structure connected by graphene units (Fig. 2c). The wall of the CANG is thin and transparent, which consists of only few layers of graphene sheets (Fig. 2d). Both TEM and SEM images display the very clean surface almost free of any particles, suggesting that the residues of Al and Co precursors were removed entirely. The high angle annular dark field (HAADF)-scanning transmission electron microscopy (STEM) image reconfirms the 3D foam-like and porous structure (Fig. 2e). Both the elemental mapping analysis of CANG by STEM (Fig. 2f) and energy dispersive X-ray spectroscopy (EDX) (Fig. S1, ESI†) elucidates the presence of C, N, Co, and Al element. Moreover, the distribution of Al and Co is as homogeneous as those of C and N, implying that Al and Co have been successfully doped into the carbon matrix of graphene.

The structure and composition of the CANG were further examined by X-ray diffraction (XRD), Raman spectroscopy, physical adsorption, and X-ray photoelectron spectroscopy (XPS), moreover, compared with those of CNG and ANG. As seen from Fig. 3a, their XRD patterns exhibit the two identical broad diffraction peaks of C (002) and C (100), respectively. The XRD pattern of CANG is free of Al- and Co-related crystalline diffraction peaks, further validating the clean surface of the graphene sheet. All of their Raman spectra exhibit the two peaks positioned at 1350 cm^{-1} and 1594 cm^{-1}, which are assigned to the D and G band peaks of graphene,[36] respectively (Fig. 3b). As is known, the G band results from the in-plane vibration of sp^2-hybridized C, and the D band stems from the edge or the defect of graphene.[37] The ratio of their intensity at the fitted D band to G band (I_D/I_G) (Fig. S2†) can reflect the structural integrity of graphene. As shown in Fig. 2b, CANG delivers the slightly higher I_D/I_G value (1.95) than those of CNG (1.9) and ANG (1.88), indicating that CANG features the slightly more defects than CNG and ANG, due most likely to the introduction of double metal heteroatoms. The nitrogen adsorption–desorption isotherm reveals that CANG has a BET surface area of 253 $m^2\ g^{-1}$ (Fig. 3c), which is close to that of ANG (257 $m^2\ g^{-1}$) and CNG (189 $m^2\ g^{-1}$), respectively. The pore-size distribution curves indicate that they possess the basically identical pore structure (Fig. S3, ESI†), and the mesopore contributes most of the surface area. Their chemical compositions were further estimated by XPS, shown in Fig. S4a, ESI.† It can be found that CANG displays the Al and Co peaks besides C, N, and O, evidencing the

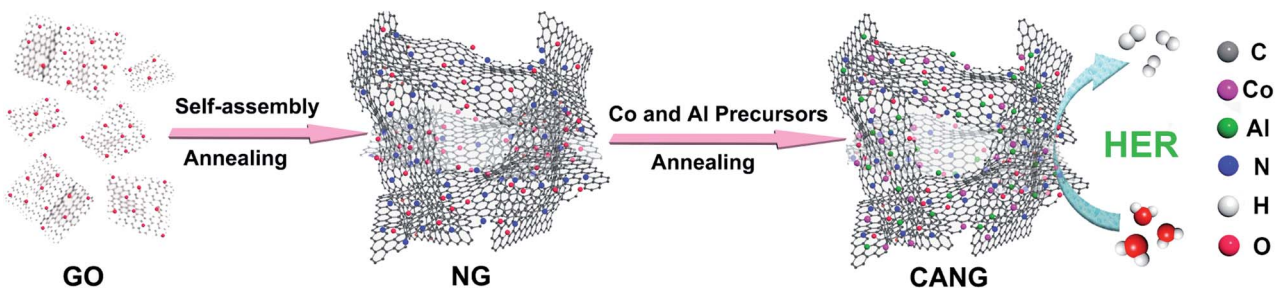

Fig. 1 Schematic illustration of the fabricating process of CANG.

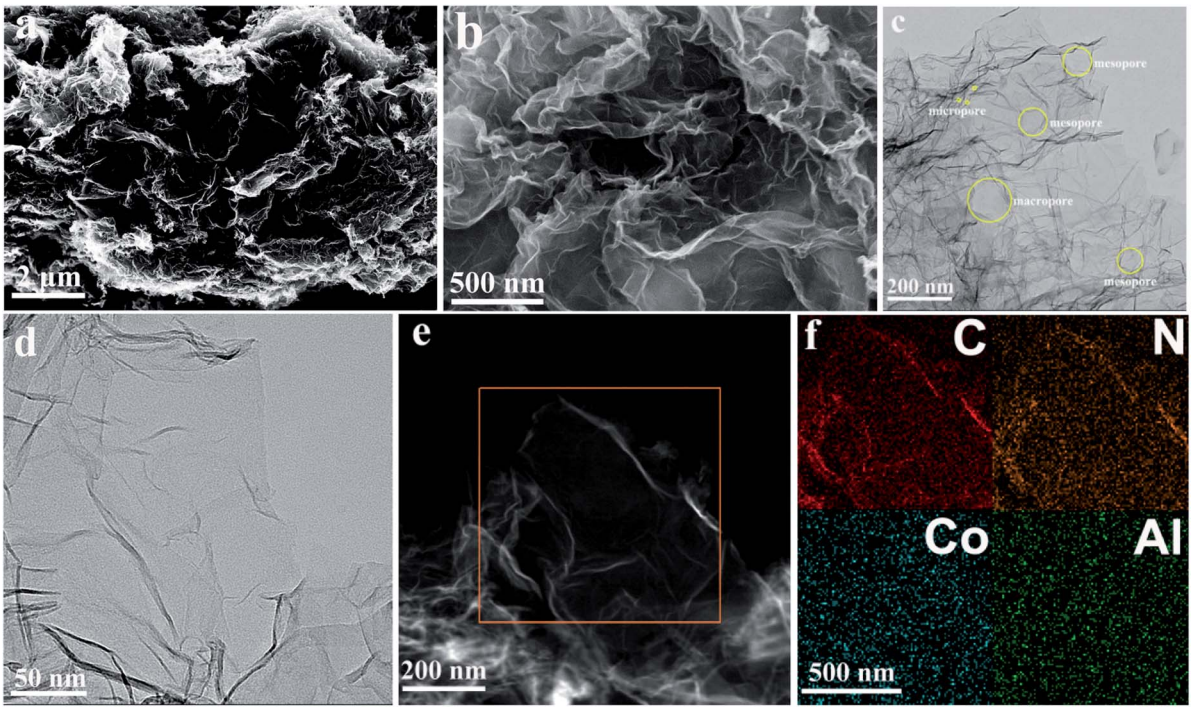

Fig. 2 The SEM (a and b), TEM (c and d), HAADF-STEM images (e), and the corresponding elemental mapping (f) of CANG.

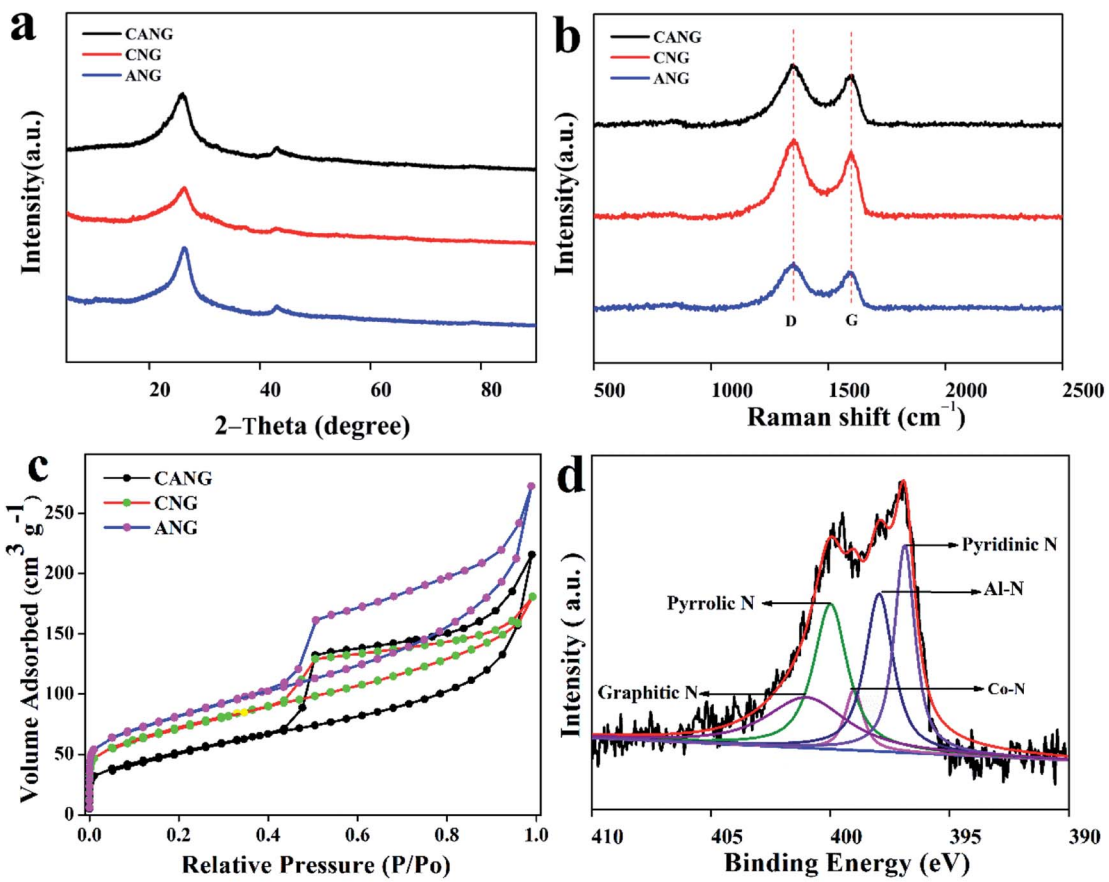

Fig. 3 (a) XRD patterns, (b) Raman spectroscopy, (c) N_2-adsorption isotherm of and N 1s XPS (d) characterization of CANG.

successful doping of Al and Co. The amounts of Al and Co in CANG are 0.51 at% and 2.18 at%, respectively, very close to those in CNG and ANG.[33,34] The Al 2p and Co 2p fine XPS of CANG showed the pronounced Al $2p_{3/2}$, Co $2p_{1/2}$, and Co $2p_{3/2}$ peaks (Fig. S4b and c, ESI†). Particularly, the high resolution N1s XPS of CANG can be deconvoluted into the clear Co–N and Al–N peaks besides the conventional pyridinic, pyrrolic and graphitic N (Fig. 3d), however, those of CNG and ANG merely show the individual Co–N peak and Al–N peak (Fig. S5, ESI†), implying the possible existence of Co–N–Al structure in CANG.

3.2 The electrocatalytic HER performance of CANG

The electrocatalytic performance of CANG for HER was firstly assessed in an acid media (0.5 M H_2SO_4) using a three-electrode electrochemical cell. The mass loading of catalysts on working electrode maintained at 0.28 mg cm^{-2} (geometrical area). The potentials against SCE were referenced to reversible hydrogen electrode (RHE). For comparison, the electrocatalytic HER performance of CNG and ANG were also measured, and benchmark to the commercial Pt/C catalyst (20 wt%). The HER activity of a catalyst is generally evaluated by the overpotential (η_{10}) needed to achieve the current density of 10 mA cm^{-2} from the linear sweep voltammetry (LSV) curves. As seen from Fig. 4a, the η_{10} of CANG is only 105 mV, which is much smaller than those of CNG (173 mV) and ANG (362 mV), respectively. The Tafel plot is a powerful metric to assess the HER performance as well as an indicator of reaction pathway. The CANG gives the Tafel slope of 81.5 mV dec^{-1} (Fig. 4b), much smaller than those of CNG (100 mV dec^{-1}) and ANG (181 mV dec^{-1}) as well. The Tafel slope ranges between 40 and 120 mV dec^{-1}, indicating that CANG catalyses the HER through the Volmer–Heyrovsky mechanism, which involves the fast release of a proton followed by a rate-limiting step of electrochemical recombination with an extra proton.[27] The ECSA and TOF were further used to evaluate the intrinsic activity of the catalysts, as shown in Fig. S6, ESI.† CANG displays the ECSA of 48 m^2 g^{-1} and the TOF of 0.3 s^{-1}, which are several times to those of CNG (21 m^2 g^{-1}, 0.05 s^{-1}) and ANG (10.7 m^2 g^{-1}, 0.02 s^{-1}), respectively. The electrochemical impedance spectroscopy (EIS) discloses that CANG holds the lowest charge-transfer resistance (Fig. S7, ESI†). All the above electrochemical parameters demonstrated the same result that CANG bears significantly better HER activity than CNG and ANG in acid condition. Specially, to achieve the high current density of 100 mA cm^{-2}, the overpotential (η_{100}) needed by CANG (197 mV) is very close to that of Pt/C (153 mV). As is known that the half reaction (OER) on the counter electrode of HER is more efficient in alkaline condition.[38–40] Therefore, the electrocatalytic HER activity of CANG in alkaline media (1 M KOH) was also considered (Fig. 4c and d). Similarly, CANG exhibits the smallest η_{10} (270 mV) and Tafel slope (120 mV dec^{-1}) among the three catalysts, elucidating the best HER activity of CANG in alkaline condition as well. In both acidic and alkaline electrolyte, the HER activity of CNG is higher than that of ANG, which implies that Co heteroatom plays the more vital role than Al in electrocatalyzing HER, however, the introduction of Al can greatly boost the HER activity of CNG. Although slightly inferior to Pt/C, CANG still shows the better HER activity than most of the Co–N–C catalysts reported in literature (Tab. S1, ESI†). The electrochemical stability tests

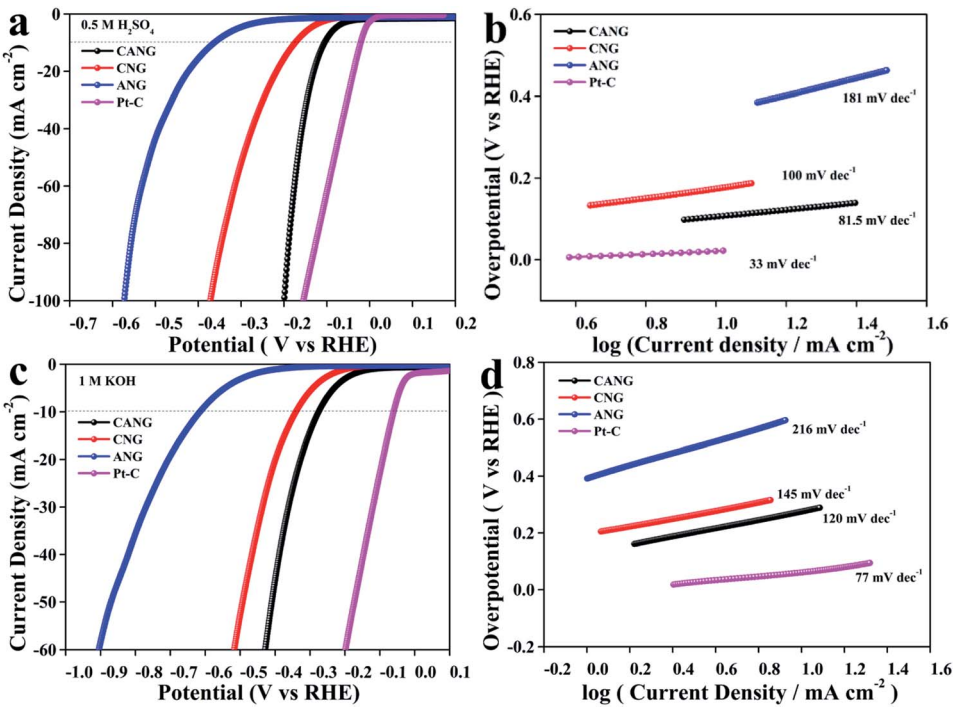

Fig. 4 Electrocatalytic HER activity of CANG in acidic (a and b) and alkaline (c and d) electrolyte. (a and c) LSV curves, (b and d) Tafel plots. Catalysts loading: 0.28 mg cm^{-2}, scan rate: 10 mV s^{-1}.

were evaluated by the LSV plot experienced 20 000 CV cycles and *i–t* curve (Fig. S8, ESI†). It can be seen that, CANG displays the excellent cyclic stability in both acidic (Fig. S8a and b†) and alkaline media (Fig. S8c and d†). Unfortunately, in neutral media (1 M phosphate buffer solution), CANG shows the same poor HER activity (Fig. S9, ESI†) as CNG and ANG. The ORR performance of CANG was considered as well (Fig. S10, ESI†). As compared with that of ANG, CANG bespeaks the degraded ORR activity, signifying that the introduction of Co can't improve the ORR activity of ANG.

To further understand the nature of active site of CANG, thiocyanate ions (SCN^-) test was performed. SCN^- is well known to poison the metal active centre in acidic condition.[41] As shown in Fig. S11, ESI,† after introducing SCN^- into the electrolyte, the η_{10} of CANG and CNG increases by 30 mV and 40 mV, respectively, however, that of ANG nearly keeps unchanged. This result evidences that the metal active centre in CANG is Co. In addition, the HER activity of CANG fabricated at various annealing temperatures were investigated (Fig. S12, ESI†). The contents of Co, Al and N in these CANG materials were determined by XPS (Tab. S2, ESI†). It was found that, the content of Co delivers the best relevance with their HER activities, further confirming the Co active centre in CANG. Admittedly, Al is not the active centre of CANG, however, it can greatly enhance the HER activity of Co active centre (Co–N–C). Based on these facts, it is inferred that the Co–N–Al structure is possibly the active centre of CANG.

3.3 The DFT calculation

DFT calculation was finally carried out to uncover the mechanism of Al-boosting the HER activity of CNG. The Co–N–C, Al–N–C and Co–N–Al structure were choose as the active centres of CNG, ANG and CANG, respectively. Their structural models can be found in Fig. S12, ESI.† The HER activity is evaluated by a three-state diagram involving H^+ (initial state), H* (intermediate state), and $\frac{1}{2}H_2$ (final state). The Gibbs free energy of adsorption under room temperature and 1.23 V electric-potential was derived based on Norskov's scheme.[42] Theoretically, an ideal HER electrocatalyst should feature a moderate free energy for H adsorption ($\Delta G(H^*)$) and desorption simultaneously.[27] Their free energy diagrams were shown in Fig. 5.

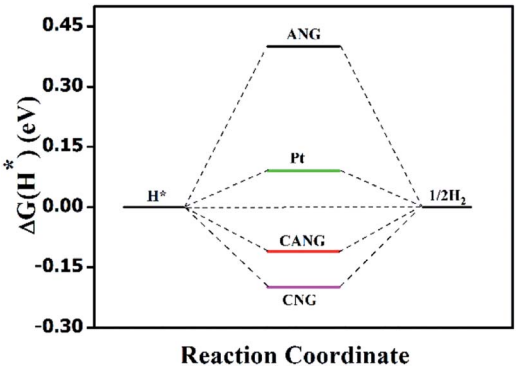

Fig. 5 Free energy diagrams of HER for active centre of Pt, CNG, ANG, and CANG by DFT calculations.

Clearly, ANG shows the highest positive $|\Delta G(H^*)|$ (0.4 eV), representing the lowest HER activity, which results from the strong hydrogen adsorption on N atom. CNG displays the relatively low $|\Delta G(H^*)|$ of 0.2 eV, due to the moderate hydrogen adsorption on Co atom. Interestingly, CANG manifests the lowest $|\Delta G(H^*)|$ of 0.11 eV, which is very close to that of Pt (0.09 eV), hinting its remarkable potentials in electrocatalyzing HER. The introduction of Al enables the $|\Delta G(H^*)|$ of Co–N–C to decrease from 0.2 eV to 0.11 eV, which may be the intrinsic reason of Al-boosting the HER activity of Co–N–C.

4. Conclusions

In summary, we proposed for the first time a Co, Al, and N tridoped graphene with robust 3D hierarchically porous structure. As an electrocatalyst for HER, this material exhibited outstanding HER activity in both acidic (η_{10} = 105 mV) and alkaline (η_{10} = 270 mV) electrolyte. Very interestingly, it was found that the introduction of Al heteroatom can notably promote the HER performance of Co–N–C catalyst. The principle developed here, Al-boosting the HER activity of Co–N–C catalysts, will provide new guidance to design advanced carbon materials with inexpensive metals for fuel cell, water-splitting and other electrochemical devices.

Conflicts of interest

There are no conflicts to declare.

Acknowledgements

This work is financially supported by the Natural Science Foundation of Jiangsu Province, China (BK20161191), the Project of Jiangsu Key Laboratory of Advanced Catalytic Materials and Technology, the Advanced Catalysis and Green Manufacturing Collaborative Innovation Centre of Jiangsu Province, and Natural Science Foundation of China (21775013).

Notes and references

1 I. Roger, M. A. Shipman and M. D. Symes, *Nat. Rev. Chem.*, 2017, **1**, 0003.
2 F. Díaz-González, A. Sumper, O. Gomis Bellmunt and R. Villafáfila Robles, *Renewable Sustainable Energy Rev.*, 2012, **16**, 2154.
3 Y. J. Sa, S. Park, G. Y. Jung, T. J. Shin, H. Y. Jeong, S. K. Kwak and S. H. Joo, *ACS Catal.*, 2019, **9**, 83.
4 Y. Jiao, Y. Zheng, M. T. Jaroniec and S. Z. Qiao, *Chem. Soc. Rev.*, 2015, **44**, 2060.
5 Y. Zheng, Y. Jiao, M. Jaroniec and S. Z. Qiao, *Angew. Chem.*, 2015, **54**, 52.
6 C. Tang, L. F. Gan, R. Zhang, W. B. Lu, X. E. Jiang, A. M. Asiri, X. P. Sun, J. Wang and L. Chen, *Nano Lett.*, 2016, **16**, 6617.
7 E. Skulason, G. S. Karlberg, J. Rossmeisl, T. Bligaard, J. Greeley, H. Jonsson and J. K. Norskov, *Phys. Chem. Chem. Phys.*, 2007, **9**, 3241.

8 S. A. Grigoriev, P. Millet and V. N. Fateev, *J. Power Sources*, 2008, **177**, 281.
9 Q. Gao, W. Zhang, Z. Shi, L. Yang and Y. Tang, *Adv. Mater.*, 2018, **30**, 1802880.
10 L. Pan, Y. Li, S. Yang, P. Liu, M. Yu and H. Yang, *Chem. Commun.*, 2014, **50**, 13135.
11 Y. Zhu, G. Chen, Y. Zhong, W. Zhou and Z. Shao, *Adv. Sci.*, 2017, **5**, 1700603.
12 W. Chen, J. T. Muckerman and E. Fujita, *Chem. Commun.*, 2013, **49**, 8896.
13 P. Xiao, W. Chen and X. Wang, *Adv. Energy Mater.*, 2015, **5**, 1500985.
14 Y. Li, F. Chu, Y. Bu, Y. Kong, Y. Tao, X. Zhou, H. Yu, J. Yu, L. Tang and Y. Qin, *Chem. Commun.*, 2019, **55**, 7828.
15 Y. Guo, T. Park, J. W. Yi, J. Henzie, J. Kim, Z. Wang, B. Jiang, Y. Bando, Y. Sugahara, J. Tang and Y. Yamauchi, *Adv. Mater.*, 2019, **31**, 1807134.
16 C. Xia, H. Liang, J. Zhu, U. Schwingenschlögl and H. N. Alshareef, *Adv. Energy Mater.*, 2017, **7**, 1602089.
17 W. Cui, Q. Liu, N. Cheng, A. M. Asiri and X. Sun, *Chem. Commun.*, 2014, **50**, 9340.
18 X. Wang, G. Sun, P. Routh, D. H. Kim, W. Huang and P. Chen, *Chem. Soc. Rev.*, 2014, **43**, 7067.
19 H. Liu, Y. Liu and D. Zhu, *J. Mater. Chem. A*, 2011, **21**, 3335.
20 U. Martinez, S. K. Babu, E. F. Holby, H. T. Chung, X. Yin and P. Zelenay, *Adv. Mater.*, 2019, **31**, 1806545.
21 M. Zhang, Q. Dai, H. Zheng, M. Chen and L. Dai, *Adv. Mater.*, 2018, **30**, 1705431.
22 S. Chao and M. Gen, *Int. J. Hydrogen Energy*, 2016, **41**, 12995.
23 A. Morozan, V. Goellner, Y. Nedellec, J. Hannauer and F. Jaouen, *J. Electrochem. Soc.*, 2015, **162**, H719.
24 L. Zhang, W. Liu, Y. Dou, Z. Du and M. Shao, *J. Phys. Chem. C*, 2016, **120**, 29047.
25 C. Deng, K. H. Wu, J. Scott, S. Zhu, X. Zheng, R. Amal and D. W. Wang, *ACS Appl. Mater. Interfaces*, 2019, **11**, 9925.
26 Z. Zhang, S. Yang, M. Dou, J. Ji and F. Wang, *Int. J. Hydrogen Energy*, 2017, **42**, 4193.
27 Z. Wang, X. Hao, Z. Jiang, X. Sun, D. Xu, J. Wang, H. Xia, F. Meng and X. Zhang, *J. Am. Chem. Soc.*, 2015, **137**, 15070.
28 H. Jin, J. Wang, D. Su, Z. Wei, Z. Pang and Y. Wang, *J. Am. Chem. Soc.*, 2015, **137**, 2688.
29 X. Ma, X. He and T. Asefa, *Electrochim. Acta*, 2017, **257**, 40.
30 T. Sun, J. Dong, Y. Huang, W. Ran, J. Chen and L. Xu, *J. Mater. Chem. A*, 2018, **6**, 12751.
31 S. Wang, Y. Qin, Y. Liu, F. Chu, Y. Kong and Y. Tao, *J. Electrochem. Soc.*, 2017, **164**, F1110.
32 S. Li, H. Li, S. Huang, Q. He and L. Hou, *Energy Technol.*, 2019, **7**, 1800757.
33 Y. Qin, H. H. Wu, L. Zhang, X. Zhou, Y. Bu, W. Zhang, F. Chu, Y. Li, Y. Kong, Q. Zhang, D. Ding, Y. Tao, Y. Li, M. Liu and X. C. Zeng, *ACS Catal.*, 2019, **9**, 610.
34 S. Wang, L. Zhang, Y. Qin, D. Ding, Y. Bu, F. Chu, Y. Kong and M. Liu, *J. Power Sources*, 2017, **363**, 260.
35 Y. Qin, J. Yuan, J. Li, D. Chen, Y. Kong, F. Chu, Y. Tao and M. Liu, *Adv. Mater.*, 2015, **27**, 5171.
36 S. Li, C. Cheng, H. W. Liang, X. Feng and A. Thomas, *Adv. Mater.*, 2017, **29**, 1700707.
37 Z. Liu, K. Parvez, R. Li, R. Dong, X. Feng and K. Müllen, *Adv. Mater.*, 2015, **27**, 669.
38 J. Jin, X. Liu, Y. Jiao, A. Vasileff, Y. Zheng and S. Qiao, *Nano Energy*, 2018, **53**, 690.
39 Y. Luo, X. Li, X. Zou, F. Kang, H. M. Cheng and B. Liu, *ACS Nano*, 2018, **12**, 4565.
40 D. Hou, S. Zhu, H. Tian, H. Wei, X. Feng and Y. Mai, *ACS Appl. Mater. Interfaces*, 2018, **10**, 40800.
41 H. W. Liang, S. Brüller, R. Dong, J. Zhang, X. Feng and K. Müllen, *Nat. Commun.*, 2015, **6**, 7992.
42 J. K. Nørskov, T. Bligaard, A. Logadottir, J. R. Kitchin, J. G. Chen, S. Pandelov and U. Stimming, *J. Electrochem. Soc.*, 2005, **152**, J23.